Improving the ion current density distribution from a gridless ion source by optimising the orientation.

Henrik Fabricius

DELTA Light & Optics
Hjortekaersvej 99, DK-2800 Lyngby, Denmark
Division of DELTA Danish Electronics Light & Acoustics
Affiliated to the Danish Academy of Technical Sciences

ABSTRACT

A Mark II gridless ion source and a HCES5000 hollow cathode electron source are used for ion assisted deposition (IAD) of dense coatings. It is possible to check the ion beam profile with a beam probe translated at a right angle to the beam axis. By rotating the probe it is possible to eliminate the contribution from charge exchange ions and to estimate the mean free path of the energetic ions. The beam intensity is expressed as a polynomial in cosine to the angle between the ion track and the beam axis and we derive mathematical equations to describe the resulting distribution of ion current density on a flat and on an umbrella shaped substrate holder. A grid of target points is introduced immediately in front of the holder and in turn we aim the ion gun towards each of these. In each case, we calculate the mean ion current density and the variance across the rotating substrate holder. Finally, we use the obtained maps to optimise the orientation of the ion gun.

Keywords: IAD, ion current profile, ion current density, ion gun orientation, gridless ion source, mean free path

1. INTRODUCTION

Optical coatings are produced by deposition of highly pure starting materials in vacuum systems that reach base pressures of less than 10^{-6} mbar. Hard durable surface coatings can be obtained by electron gun deposition of metal-oxides like titanium dioxide, TiO_2, zirconium dioxide, ZrO_2, hafnium dioxide, HfO_2 and quartz, SiO_2[1,2]. It is necessary to deposit the thin films in a reactive oxygen atmosphere to compensate for a tendency of the metal-oxides to dissociate as they shift from the solid state to the gas phase[3]. Unfortunately the presence of a gas during the deposition is detrimental to a dense microstructure[1,4,5], and although the coatings are hard, the layers tend to be relatively porous. To produce precision coatings like the gradient index filters from DELTA light & Optics[6,7] it is necessary to increase the density of the layers during the deposition to stabilize the parameters and to enable a computer controlled deposition of coatings with a complicated code.
Ion assisted deposition (IAD) has become established for making optical coatings denser to stabilize their optical parameters[1,2,4,5,8]. In the autumn of 1995 we installed a gridless Mark II ion gun and a hollow cathode electron source HCES5000 from the Commonwealth Scientific Corporation, CSC, to be used with two electron guns in a Balzers BAK640 vacuum chamber. A year later we furthermore replaced the stainless Steel anode with a new water-cooled anode from CSC to protect the magnet in the end-Hall source against demagnetization caused by the heat from an un-cooled anode. The ion source was mounted at the base-plate of the vacuum chamber and in an off axis position to allow for transmission of light for the optical monitoring system (see figure 1). The paper deals with the subject of optimizing the orientation of the ion gun to obtain an even distribution of the ions impinging on the substrates.

2. THE ION GUN AND THE HOLLOW CATHODE

The functional principle of the end-Hall source was described in details by Kaufman et al.[9,10,11] and recently to some extend by Willey[4,12,13]. It produces a broad beam of energetic ions well suited to cover large substrate holders as used in a production environment. The gas to be ionized is admitted through the anode at a controlled flow rate. Depositing metal-oxides the gas is pure oxygen and the anode is made of stainless steel. Electrons from an electron source bombard the gas as a positive DC-voltage is applied to the anode and an ionization of the gas occurs at a sufficient high voltage and flow of oxygen. A primarily axial magnetic field in the anode region enhances the affectivity of the electrons and some of them strike the oxygen molecules on their path towards the anode. Some of these collisions produce ions. Most of the ionizing collisions with neutrals occur in the region surrounded by the anode[9,10]. The mixture of electrons and ions in the discharge region forms a conductive gas, or plasma. Most of the potential variation across the plasma is found in the axial direction parallel to the magnetic field[9,10,11]. The ions formed are accelerated by the electric field and they form a divergent beam.
In most systems the cathode is formed by a simple hot cathode filament placed approximately 5cms in front of the anode. However, the lifetime of such a hot filament placed in the path of the ion beam is limited to be between four and nine hours

Part of the EUROPTO Conference on Advances in Optical Interference Coatings
Berlin, Germany • May 1999
SPIE Vol. 3738 • 0277-786X/99/$10.00

when the gas is oxygen and the cathode contaminates the thin-film as it degrades. At DELTA Light & Optics we use a more advanced type of neutralizer - a so-called Hollow Cathode Electron Source (HCES) - which contaminates less and which can be operated for several hundred hours without any service. Furthermore it is located outside the ion beam which eases the access to the anode which should be cleaned subsequently to each coating run to remove oxides formed on the surface by reaction with the oxygen.

A hollow cathode is a small discharge chamber with a small aperture in the front end (keeper) from which electrons are drawn to the ion beam. The process gas in the HCES is pure argon and the hollow cathode requires an internal pressure of 1 – 10 Torr to operate. The internal plasma serves to heat a tantalum insert, which works in turn as a thermal electron emitter. In our coating system argon is supplied at a ratio of around 15 SCCM. One of the drawbacks of the HCES5000 is the increased pressure in the coating machine. The partial pressure of argon is 5.5E-5 mbar at this flow rate. It is possible to reduce the argon flow towards 10 SCCM. However, in this case the coupling voltage between the cathode and the ion beam increases. This is a disadvantage because there is some sputtering from near the aperture in the tantalum keeper and the rate of this sputtering process increases with the coupling voltage. As a consequence the service intervals would be shortened and the contamination from the HCES increased. The main drawback of the HCES5000 is that it imposes a limit on the anode current for the Mark II ion gun. To achieve both charge and current neutralization it is recommended that the current in the neutralizer is 10 – 15 percent higher than the anode current in the Mark II. This limits the maximum anode current in the MARK II ion gun to about 4.2 amps.

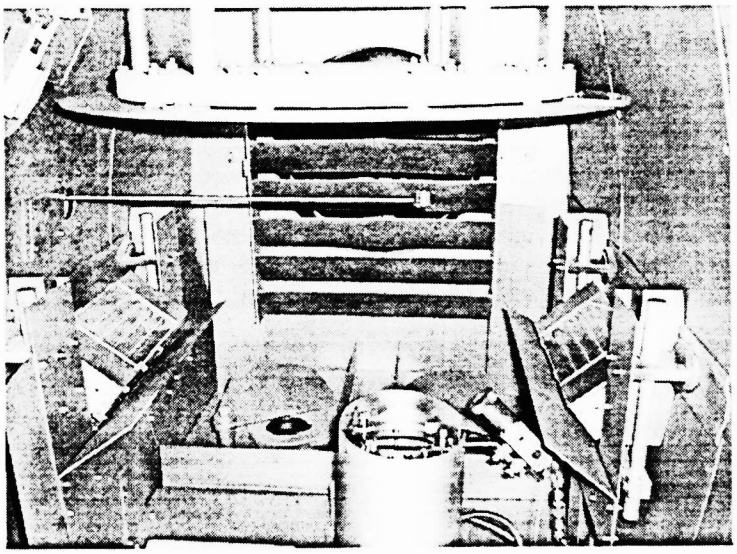

Figure 1 Photo of the vacuum chamber with the two electron – guns (in the back ground), the Mark II ion gun (at the front) and the HCES5000 Hollow Cathode Electron Source (mounted on the right side of the ion gun). The sliding planar beam probe is introduced from the left.

The electrons from the hollow cathode both serve to ionize the oxygen and to neutralize the ion beam. The neutralization is needed to avoid charging of non-conducting target surfaces and succeeding arching which imposes damages to them. Furthermore, the density of the ion beam is so high that the repulsion of like charges would spread them excessively without the presence of the neutralizing electrons. Neutralization does not refer to the actual recombination of electrons and positive ions, which is actually a negligible process in most ion beam processes. Neutralization means establishing a charge balance between the positive ions and the negative electrons[9]. This balance can be between the densities of charges in the ion beam in which case it is called charge neutralization, or it can be a balance between the arrival rates of electrons and ions on the target in which case it is called current neutralization.

3. MEAN FREE PATH

The ion beam is rotational invariant regarding the beam axis. Therefore it is possible to check the profile with an ion beam probe translated at a right angle to the beam axis. Figure 1 is a picture of the vacuum-chamber with the gridless ion-source, the HCES, a flat substrate holder and a sliding planar beam probe from CSC. It is possible to slide the probe without affecting the pressure in the vacuum system as it is introduced through a unit with differential pumping. The ion collecting area of the probe is 1 cm^2. A B&O SN16 power supply was used to introduce a bias voltage to repel electrons from the sensing surface. The probe housing was connected to the chamber ground, and the ion current was measured indirectly through the voltage across a resistance of 100 ohm. The voltage was measured with a Metrix MX573 meter Arepa calibrated on the 1999-02-11.The orientation of the probe was controlled by mounting a pointer to the end of the probe, and by application of a fixed scale.

Initially the probe was placed right in front of the ion gun. The exact centre of the beam was easily found from a parabolic fit of data collected across the centre of the beam. The centre appeared to be within 3mms from the point deduced from the mechanical alignment (A disc with a long rod in the centre is fixed to the front of the ion gun when the orientation is changed). In this position the distance to the emission-point of the ion source was 316mm. Turning on the HCES5000 it was

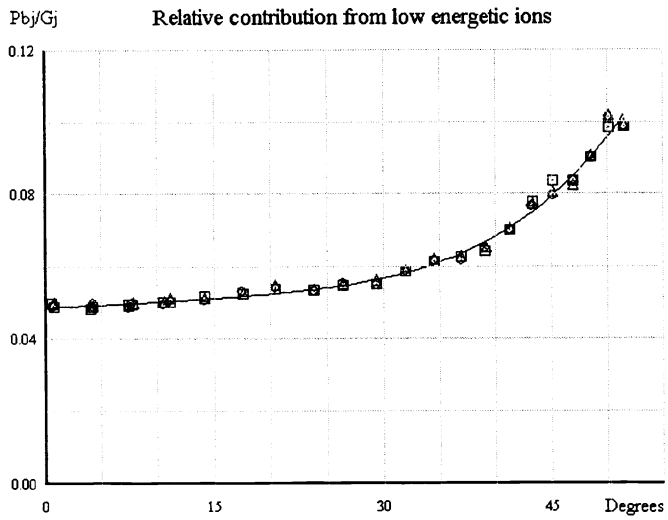

Figure 2 It is possible to isolate the contribution from the low energy charge exchanged ions, by rotating the planar probe. The fraction of low energy ions increases at angles beyond 40 degrees because the less energetic ions tend to be deflected away from the dense central portion of the ion beam[9].

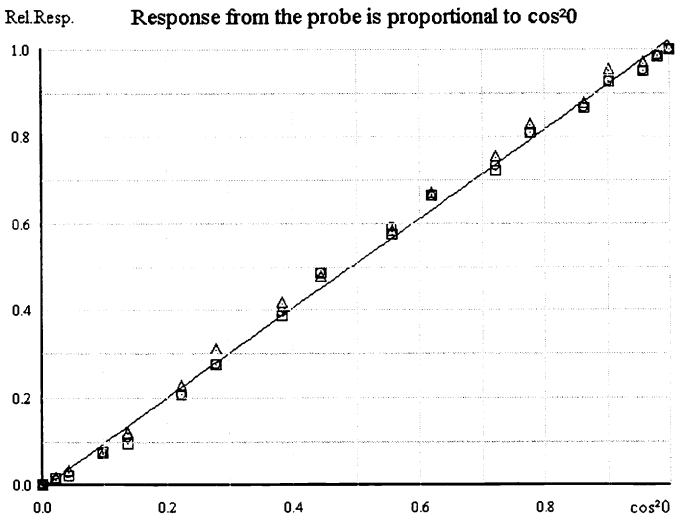

Figure 3 The response from the planar ion beam probe from Commonwealth Scientific Corporation is proportional to $\cos^2\theta$

necessary to introduce a bias-voltage on the probe, which had to be as negative as the HCES keeper voltage, to get a zero response from the probe. In this situation where the ion gun was not yet turned on, the keeper voltage was –45 volts.

However, as soon as the ion gun was turned on the keeper voltage dropped to around -18 volts. The rest of the measurements were made with a bias voltage of –28 volts corresponding to the bias voltage applied by the Millatron monitor delivered with the probe.

The response from the planar probe depends on the angle of incidence of the ions. The sensing area is not flush with the front of the probe, and this makes it necessary to test the angular dependence of the probe prior to any other measurements. This was done, by rotating the probe at the centre of the beam. It turned out that the response from the probe was constant within ± 5 % in the angular range from 90 degrees to 270 degrees relative to normal orientation. This was also the case at any other position along the track and the constant contribution was interpreted as originating from low energy ions formed by charge exchange between the neutral background gas in the chamber and the energetic ions (see figure 2). The constant contribution from these low-energy ions was subtracted from the measurements to obtain the contribution from the energetic ions following nearby straight line trajectories from the ion source[9,10]. Figure 3 shows a plot of the relative response from the probe as function of the square of cosine to the angle. The data were collected from two rotations of the probe. It is evident that the angular dependence of the probe is approximately proportional to $\cos^2\theta$.

$$f(\theta_j) = \cos^2\theta_j = (h_i / S_j)^2 \qquad (1)$$

where h_i is the shortest distance between the probe and the emission point of the gun (here 316mm), and where S_j is the actual distance between the probe and the emission point of the ion gun.

$$S_j = [h_i^2 + (x_j - x_{jo})^2]^{1/2} \qquad (2)$$

Where x_{jo} is x_j at the center of the ion beam.

The observation that it is possible to measure the contribution from the low-energy charge exchanged ions by rotation of the probe at the sampling points gives us an interesting possibility to estimate the mean free path of the energetic ions. Imagine that the response is measured at different distances x_j along the linear path of the sliding probe and that we call the measured responses P_j. Furthermore, please imagine that P_{jb} symbolises the average of the measured values in the sideways and backwards direction. In this case it is possible to correct the measurements for the angular dependence and the influence from the low-energetic ions by replacing P_j by G_j where

$$G_j = (P_j - P_{jb}) / f(\theta_j) \quad (3)$$

If we assume that the pumping of the background gas and the energetic gas is equally good, the following equation describes the interaction with the background gas

$$\Gamma_n / \Gamma_{no} = \exp(-S_j / \lambda_n) = G_j / (G_j + P_{jb}) \quad (4)$$

where λ_n symbolizes the mean free path.

The mean free path of energetic ions increases with their energy[14], which may depend on the angle of emission from the ion gun. Equation 4 is easily rearranged to obtain the following expression for the mean free path at the angle θ_j.

$$\lambda_n(\theta_j) = -S_j / \ln[G_j / (G_j + P_{jb})] \quad (5)$$

If we assume that the mean free path is constant in a certain angular range, the following equation should be fulfilled

$$\lambda_n = (1/N) \sum_{j=1}^{N} \lambda_n(\theta_j) \quad (6)$$

The mean free path was estimated from three series of measurements for the following conditions: MARK II ion gun : V_a = 130V, I_a = 4.18A, Flow of oxygen : 18.6 SCCM, partial pressure : 8.0E-5 mbar; HCES5000 : I_e = -4.92A, flow of argon 15 SCCM, partial pressure : 5.5E-5 mbar.

$$\lambda_n(0° \rightarrow 45°) \approx 6.533\text{m} \quad (7)$$

The energetic ions and the thermal energy neutrals mainly interact through collisions and charge exchange[14]. The speed of the background atoms and molecules is negligible compared to the speed of the beam ions. Hence the expression for the momentum-loss path length is[14]

$$\lambda_{nn} = 1 / (n_n Q_{nn}) \quad (8)$$

where n_n is the density of the background gas and Q_{nn} the momentum transfer cross section. According to the equation of state of an ideal gas the pressure is proportional to the density of molecules in the chamber, and at a pressure of one atmosphere and a temperature of 20°C the density of gas molecules is 2.5E25. This means that in our case we have

$$\text{Argon} : n_n = 2.5\text{E}25 / (\text{bar m}^3) * 5.5\text{E-}8 \text{ bar} = 1.4\text{E}18 \text{ m}^{-3} \quad (9)$$

$$\text{Oxygen} : n_n = 2.5\text{E}25 / (\text{bar m}^3) * 8.0\text{E-}8 \text{ bar} = 2.0\text{E}18 \text{ m}^{-3} \quad (10)$$

According to reference 9 the momentum transfer cross-section of the thermal energy neutrals[15] is 42E-20 m^2 for argon and 41E-20 m^2 for oxygen. However, at a collision-energy of 50eV, the value has dropped to 2.32E-20 m^2 for argon[14]. The corresponding value for oxygen is not listed. However, the cross section typically increases with the atomic number and a worst case calculation yields.

$$\lambda_{nn} = 1 / (n_n Q_{nn(\text{oxygen})} + n_n Q_{nn(\text{argon})}) > 1 / [(2\text{E}18\text{m}^{-3} + 1.4\text{E}18\text{m}^{-3}) * 2.3\text{E-}20\text{m}^2] = 12.8\text{m} \quad (11)$$

As mentioned the energetic ions also interact with the thermal-energy neutrals through charge exchange[14]. The result of such an interaction is a thermal-energy ion and an energetic neutral. If the ion and the neutral are the same atomic or molecular species, the process has a larger cross section (a larger probability of occurring) and it is then called a resonant charge exchange. However, O^+ ions in a gas of argon and O_2 do not fulfil the requirements for resonant charge exchange and the cross section is greatly reduced. According to ref 14 there is no reason to expect the charge exchange cross section to be much larger than the momentum cross section. This statement seems to agree very well with the fact that the derived value of the mean free path (Eq. 7) is half of the estimated mean free path between collisions (Eq. 11).

Figure 4 is a plot of the corrected data $G_j / (G_j + P_{jb})$ from the probe measurements as function of the distance S_j between the probe and the emission point. The dashed curve is a plot of the function $\exp[-S_j / \lambda_n(0° \rightarrow 45°)]$. It is seen that the assumption about a constant mean free path is reasonable at angles less than 40 degrees ($S_j < 41.3$cm). At larger angles the data points are all below the curve corresponding to lower values of the mean free path. This is in good agreement with measurements by Kaufman et al., which indicates a reduced ion energy, at large angles[16,17].
It is possible to use the plot to derive an expression for the mean free path as function of the angle of emission. In this case a parabolic fit appears to fit well, leading to the following expression:

$$\lambda_n(\theta_j) = -S_j / \ln[-0.682034\, S_j^2 + 0.318983\, S_j + 0.920504] \qquad (S_j \text{ in meters}) \qquad (12)$$

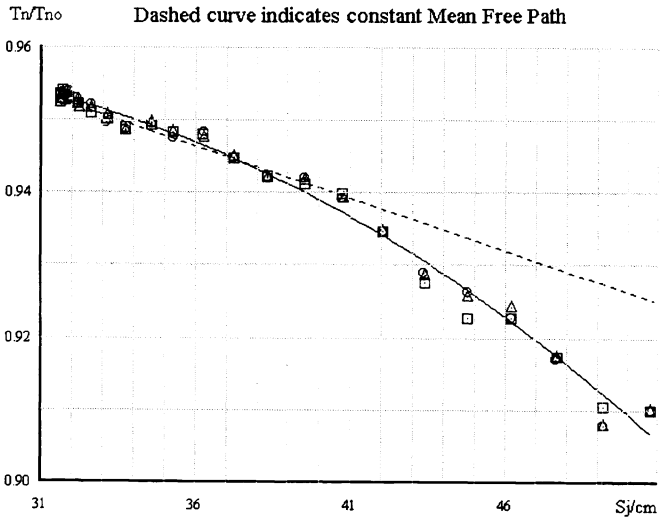

Figure 4 Plot of the corrected data $G_j/(G_j + P_{jb})$ from the probe measurements as function of the distance S_j between the probe and the emission point. Dashed curve indicates constant mean free path.

It is of course important where the emission-point is assumed to be located. In this case it was assumed that the emission point was located at the center of the anode. This seems reasonable as most of the ionizing collisions with neutrals occur in the region surrounded by the anode[9,10,11]. The calculations were repeated for other locations of the emission point. In those cases where the emission point was located at a higher position, the curves indicated the presence of increased ion energies at off axis angles. This seems to be unrealistic.
The geometry in the applied BAK640 coating machine guaranties a maximum angle of emission between the beam-axis and the most distant point on the applied substrate holder (Ø42cm) of 41 degrees. According to figure 4, it is reasonable to apply constant values for the mean free path and the mean ion energy in this case.
Never the less an attempt was made to measure the mean ion energy as function of the emission angle by sliding the planar probe in a screened steel-box. An HP6448B DC power supply (0-600V, and 0-1.5A) was used to bias the screen positively. However, the screen picked up an unacceptable fraction of the electrons from the cathode as the bias voltage was increased. It was evident from this experiment that the biased screen in a screened probe must be as small as possible to reduce the undesired influence on the plasma to an acceptable level for this type of experiment to be reliable. No further attempt was made to measure the mean ion energy as function of the exit angle because the mean free path and the mean ion energy seem to be nearly constant in the angular range of interest in the BAK640 coating machine.

4. ION BEAM PROFILE

We will now try to establish a mathematical model, which we will use to determine the ion beam profile and the ion-current density distribution on the flat and on the umbrella shaped substrate holders. In the following bold characters symbolize vectors. Figure 5 shows a schematic drawing of the system where the ion gun is placed off center in respect to a rotating flat or umbrella shaped substrate holder. The z-axis of the coordinate system we use is coinciding with the axis of the rotating substrate holder, whereas the base plate of the vacuum system forms the xy plane. The center substrate is located at

$$\mathbf{P}_h = (0, 0, h) \qquad (13)$$

The ion source is mounted on a fixed holder, which allows for adjustment of the orientation of the ion source. In the following we will assume that the center of the base plate for the ion source is fixed at the position

$$\mathbf{P}_i = (x_{io}, y_{io}, z_{io}) \qquad (14)$$

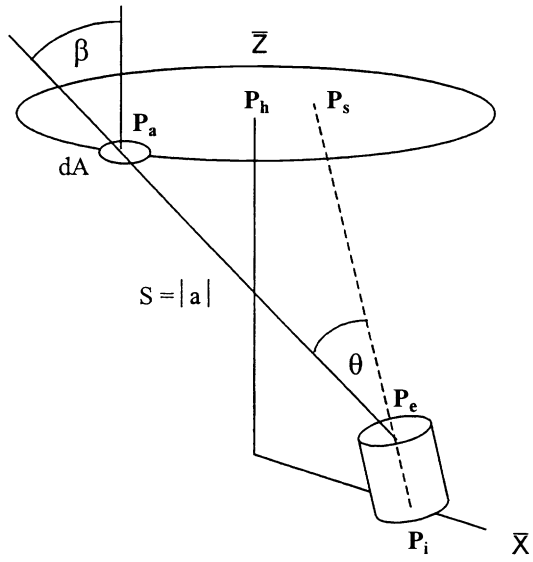

Figure 5 Schematic drawing of the system where the ion gun is placed off center in respect to a rotating flat or umbrella shaped substrate holder

and that the ion source is directed towards the point

$$\mathbf{P}_s = (x_s, y_s, h) \tag{15}$$

The directional vector in this case is given by

$$\mathbf{n}_i = (\mathbf{P}_s - \mathbf{P}_i) / | \mathbf{P}_s - \mathbf{P}_i | \tag{16}$$

The distance from the bottom of the ion source to the emission point in the center of the anode is L = 161mm – 23mm – 22/2mm = 127mm. Hence the emission point of the ion gun is placed at the position

$$\mathbf{P}_e = \mathbf{P}_i + L * \mathbf{n}_i \tag{17}$$

The angular ion emission from the ion gun is described by an expression of the following type

$$d\Phi / d\omega = \sum_{m=1}^{n} c_m \cos^m\theta \tag{18}$$

where

θ is the angle between the beam-axis and the vector **a**, which connects the center, $\mathbf{P}_a$, of a surface element, dA, on the rotating substrate holder, with the emission point of the ion gun, $\mathbf{P}_e$.

$$\cos\theta = \mathbf{a} \cdot \mathbf{n}_i / | \mathbf{a} | | \mathbf{n}_i | \tag{19}$$

$$\mathbf{a} = \mathbf{P}_a - \mathbf{P}_e \tag{20}$$

The contribution to the solid angle, dω, is given by

$$d\omega = 2\pi \sin\theta \, d\theta \tag{21}$$

The total ion emission from the gun in the angular range from zero to θ_{max} is calculated by integration

$$\Phi_{tot} = \int_0^{\theta_{max}} 2\pi \left(\sum_{m=1}^{n} c_m \cos^m\theta \right) \sin\theta \, d\theta = 2\pi \sum_{m=1}^{n} c_m (1 - \cos^{m+1}\theta_{max}) / (m + 1) \tag{22}$$

The surface element dA, which may have any orientation in respect to the ion gun is seen at a solid angle of

$$d\omega = \cos\beta * dA / S^2 \tag{23}$$

where S symbolizes the length of the vector **a**. β is the angle between the normal, $\mathbf{n}_a$, to the surface element and the directional vector **a**.

$$\cos\beta = \mathbf{a} \cdot \mathbf{n}_a / | \mathbf{a} | | \mathbf{n}_a | \tag{24}$$

It is possible to calculate the ion current density at the surface element indexed k by combining the knowledge of the mean free path in the process gas (Eqs. 4, 7 and 12) with the contents of Eqs. 18 and 23.

$$\xi_k = d\Phi_k / dA_k = d\Phi_k / d\omega_k * d\omega_k / dA_k \Rightarrow$$

$$\xi_k = \cos\beta_k * \exp(-S_k / \lambda_n(\theta_k)) / S_k^2 * \sum_{m=1}^{n} c_m \cos^m\theta_k \quad (25)$$

During the measurements where the planar ion beam probe is translated at a right angle to the beam axis and orientated towards the ion gun, $\cos\beta_k$ is equal to $\cos\theta_k$. By rearrangement of Eq. 25 we obtain the following expression, which can be used to determine the coefficients, c_m, for the polynomial that describes the angular ion emission from the ion gun

$$\sum_{m=1}^{n} c_m \cos^{(m-1)}\theta_k = \xi_k * S_k^4 / h_i^2 * \exp(S_k / \lambda_n(\theta_k)) = G_k * S_k^4 / h_i^2 * \exp(S_k / \lambda_n(\theta_k)) \quad (26)$$

where G_k symbolizes the corrected measured ion current densities as expressed by Eq. 3. Figure 6 illustrates how the coefficients were extracted by performing a Chebyshev polynomial fit. The derived expression for the angular ion emission from the investigated gun was

$$d\Phi / d\omega = 24.4989 \cos^5\theta - 75.1489 \cos^4\theta + 83.8675 \cos^3\theta - 40.2294 \cos^2\theta + 7.4705 \cos\theta \text{ Amps/str.} \quad (27)$$

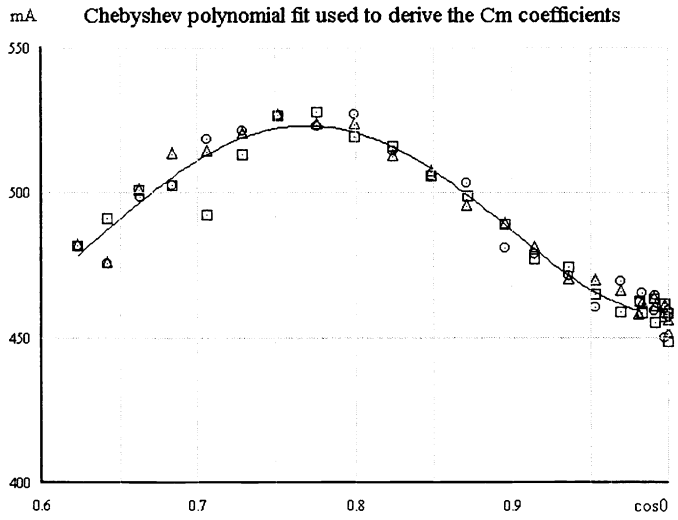

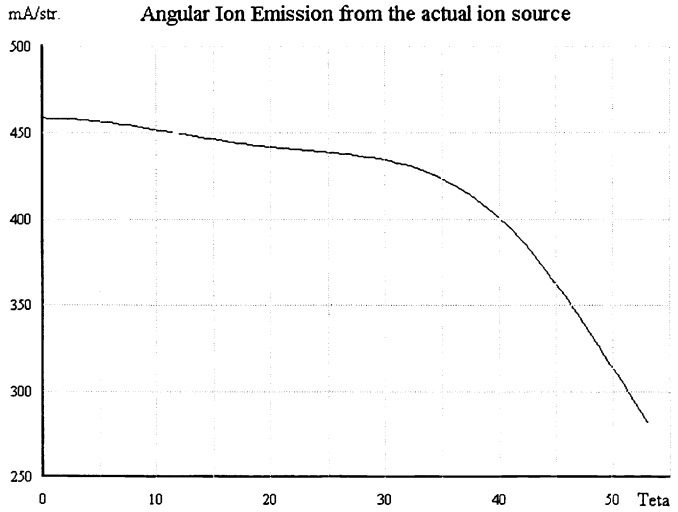

Figure 6 The coefficients c_m for equations 26 and 27 were derived by performing a Chebyshev polynomial fit. Equation 27 describes the angular ion emission from the ion gun.

Figure 7 shows the calculated angular ion emission from the tested ion source as derived from equation (27).

The markers in Figure 8 mark the measured ion current densities, G_j , as function of the position of the ion beam probe. The solid curve shows the corresponding predicted relation as obtained by insertion of the data from Eqs. 7,12 and 27 into equation 25.

Figure 7 Calculated angular ion emission from the tested ion source as derived from equation (27). The ion beam profile for a gridless ion source is often approximated by a simple $\cos^n\theta$ function[11,17]. Applying this technique to the curve shown we end up with a value of n, which is close to 1.

at an anode voltage of 130V, an anode current of 4.2 Amps, an oxygen flow of 18.6 SCCM, a cathode emission current of –4.9 Amps and an argon flow of 15 SCCM in the HCES.

Equation 22 tells us that the ion gun delivers a total ion current of 779 mA in the angular range from zero to 45 degrees, and that the value increases to 992 mA when the maximum angle is increased to 53 degrees. The calculated efficiency of the ion gun agrees well with the data from CSC[9,10,16].

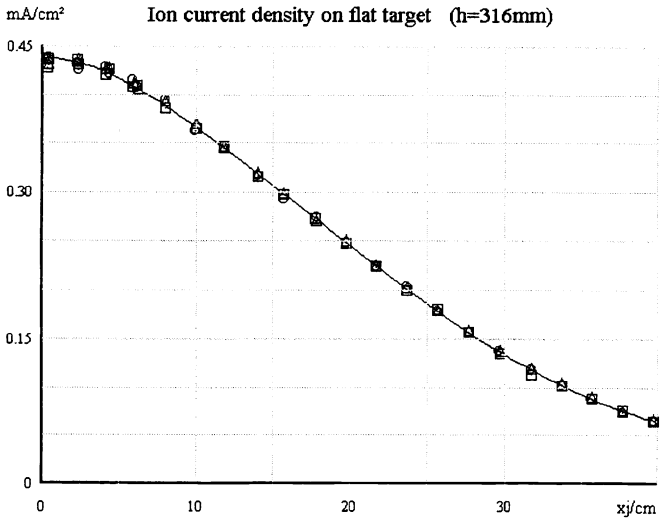

The ion beam profile for a gridless ion source is often approximated by a simple $\cos^n\theta$ function[11,17]. Experimentally, values of n usually fall in the range from 1 – 5 for the type of gridless source described, and a value of around 3 is found for the curves in references 11 and 17. A simple approximation is obtained by localizing the half value points of the profile. Applying this technique to the curve shown in figure 7 we end up with a value of n, which is close to 1.

Figure 8 The markers indicate the measured ion current densities, G_j , as function of the position of the ion beam probe. The solid curve shows the corresponding predicted relation as obtained by insertion of the data from Eqs. 7, 12 and 27 into equation 25.

As we have seen, the mean free path is in the order of 6.5 meter, which is much larger than the distance between the ion gun and the probe. Hence it is less likely that the low order could be explained by the interaction with the background gas or the argon from the HCES. Insufficient space neutralization would spread the ions due to the repulsion of like charges. However, this is not really a likely explanation as the emission current from the hollow electron source was 17 percent larger than the anode current during the test-runs, and we did not observe any arching or damages to coatings made with the ion gun system. A more likely explanation would be a weakened magnetic field in the anode region.

The magnetic field in the center of the exit plane (outer surface of the front support plate) was measured with a hand held Gauss/Tesla Meter (F. W. Bell model 4048, NPL calibrated on 1998-03-26), which was zeroed with the supplied zero Gauss chamber. The strength of the magnetic field was 39.8 Gauss. According to the manual for the ion gun[16] the reading should be in the 40 – 50 Gauss range if no significant degradation has occurred. A weakened magnet may be the explanation why we observe the low order, and it will be changed as soon as possible. It is important to notice that the magnet was used with a water-cooled anode. It is not likely that the magnet has been heated to a level where demagnetization may occur. Therefore, we must conclude that the magnet may have been affected when installed.

Some processes depend on the ion current density, while others depend more on the kinetic energy of the ions. In ref. 11 Kaufman et al. obtained the correction for variations of the ion energy by multiplying the measured off-axis current density by the ratio of off-axis to on-axis mean energies. At an angle of 40 degrees they used a correction factor of 0.8. As stated earlier in this paper the mean ion energy seems to be nearby constant in the angular range from zero to forty degrees in the present case where the ion beam profile is of a lower order (close to 1 as compared to 3 in ref 11).

5. OPTIMIZING THE ION CURRENT DENSITY DISTRIBUTION

The ion gun is typically positioned off axis in respect to a rotating substrate holder, and the ion current density distribution at the substrate holder is of course influenced by the orientation of the ion gun. The question is how the gun should be oriented to achieve an even ion current density distribution, a high ion current density, and a minimal sensitivity towards changes in the ion beam profile.

The average ion current density at a distance r from the center, $\xi(r)$, is found by integration in respect to the angle of rotation, α, of the rotating substrate holder

$$\xi(r) = (1/\pi) \int_0^{\pi} \cos\beta * \exp(-S / \lambda_n(\theta)) / S^2 * \Big(\sum_{j=1}^{n} c_j \cos^j\theta \Big) \, d\alpha \qquad (28)$$

where

$$S = |\mathbf{a}| \qquad (29)$$

$\cos\theta$ is given by Eq. 19 and $\lambda_n(\theta)$ is the mean free path of the ions

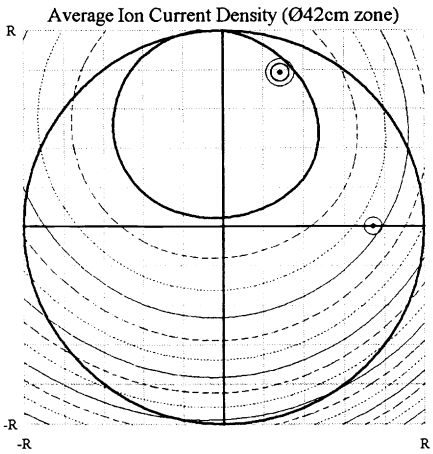

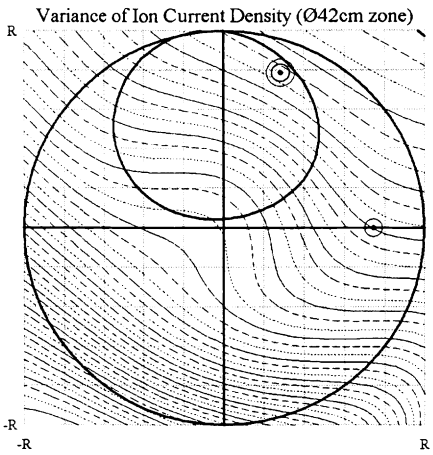

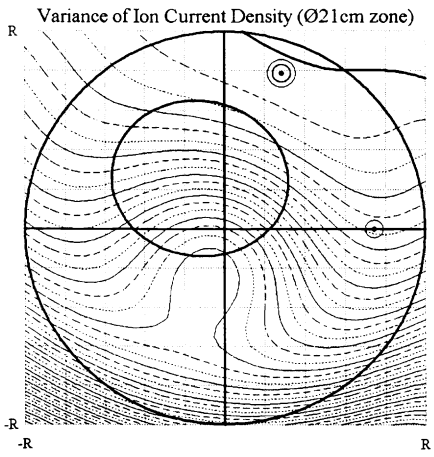

In those cases where the substrate holder is flat we have

$$\mathbf{a} = (r\cos\alpha,\ r\sin\alpha,\ h) - \mathbf{P_e} \qquad (30)$$

$$\cos\beta = h_i / S \qquad (31)$$

If the substrate holder is umbrella shaped with a bending radius, R_h, the relation changes to become

$$\mathbf{a} = (R_h \sin v \cos\alpha,\ R_h \sin v \sin\alpha,\ (h - R_h [1 - \cos v])) - \mathbf{P_e}$$

$$\cos\beta = \mathbf{a} \cdot \mathbf{n_a} / |\,\mathbf{a}\,|\,|\,\mathbf{n_a}\,| \qquad (33)$$

where

$$\mathbf{n_a} = (\sin v \cos\alpha,\ \sin v \sin\alpha,\ \cos v) \qquad (34)$$

and where the angle v is connected to the right angled distance, r, from the rotational axis to the center of the surface element dA

$$r = R_h \sin v \qquad (35)$$

The following data are valid for the configuration shown in figure 1 and drawn in figure 5: The center substrate is located at $\mathbf{P_h}$ = (0, 0, 560mm), the fixed base point of the holder for the ion gun is placed at $\mathbf{P_i}$ = (156.5mm, 0, 20mm). The radius, R, of the flat substrate-holder is 210mm and the bending radius, R_h, of the umbrella shaped holder is 631.7mm. The large solid circles in figures $9_{a\text{-}c}$, $10_{a\text{-}b}$, $12_{a\text{-}b}$ and $13_{a\text{-}b}$ marks the rim of the substrate holder. The thick solid lines symbolizes the x and the y-axis of the applied coordinate system (see figure 5) and a marker at the x-axis indicates the position, $\mathbf{P_i}$, of the holder for the ion gun.

Now, please imagine that a grid of target points is introduced immediately in front of the substrate holder and orientated in accordance with the applied coordinate system. In turn we aim the ion gun towards the different grid points, $\mathbf{P_s}$, and in each case we calculate the mean ion current density and the variance of it on the rotating substrate holder. In one type of plot we connect the target points which give the same mean ion current density on the rotating substrate holder (see the figures 9a, 10a, 12a and 13a). In another type of plot we connect the target points which give the same variance of the ion current density on the rotating substrate holder (see the figures 9b, 9c, 10b, 12b and 13b). In each plot the difference between the successive iso-curves corresponds to a relative change in the measured quantity of two percent, and the best result is set off by a thick solid curve. Hence the elliptic zones in the figures 9a, 10a, 12a and 13a indicate the coordinates the ion gun should be directed towards to maximize the mean ion current density.

Figures 9a-c Thick solid circle and lines represent the rim of a flat substrate holder and the coordinate system. Mapped parameters are the mean ion current density and the variance of the same as function of the aiming point for the tested ion gun. The zone leading to the highest ion current density is marked with a thick solid curve in each figure. The zones leading to the smallest variance are also marked with thick solid curves in the figures 9b and 9c. The double ring shaped marker highlights a target point offering a good compromise between the different preferred characteristics: high ion current density, small variance of the same and low sensitivity to changes in the ion beam profile.

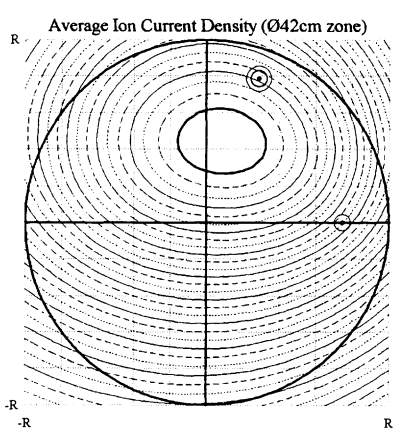

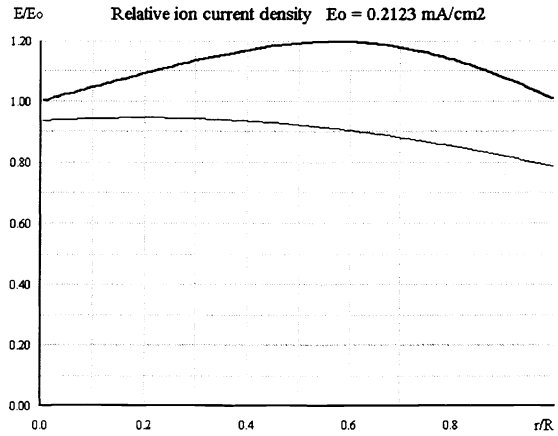

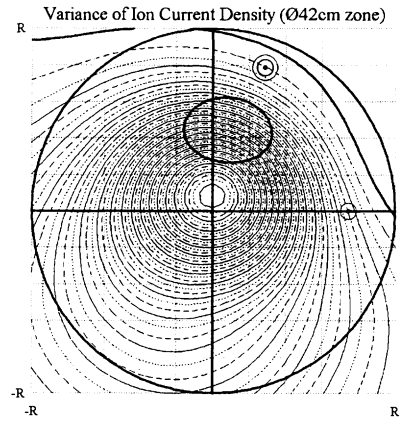

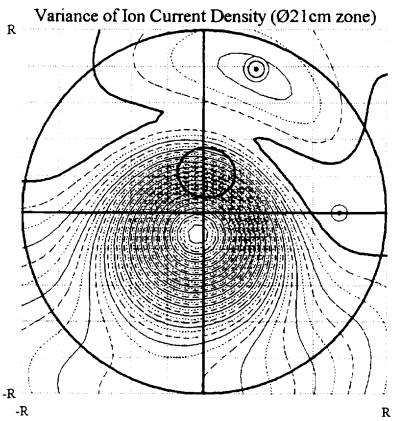

Figure 10a-c Same as figures 9a-c but in this case the ion source has a higher ordered ion beam profile ($n \approx 3$). The spacing between the curves corresponds to a change of 2 percent in the parameter

Figure 11
Curves show the predicted ion current density distribution as obtained when the ion gun is orientated towards the double ring shaped marker in the figures 9a-c and 10a-b. Thin solid curve belongs to the tested ion source (mean ion current density = $0.186 mA/cm^2$) whereas the thick solid curve belongs to the reference source (mean ion current density = $0.240 mA/cm^2$).

The thick curve is repeated in the corresponding variance plot to make it easier to identify target points both leading to a low variance and a large mean ion current density.

Figures 9a, and 9b show the results obtained for the tested ion source ($n \approx 1$) and a flat substrate holder. Figures 10a and 10b show the corresponding results obtained for a Mark II ion source with a higher ordered emission profile ($n \approx 3$), as described in references 11 and 17 and in the manual for the ion gun (from now on called the reference source).

Figures 9c and 10c are examples of plots where the magnitude and variance of the ion current density is only investigated for the central part of the substrate holder that has a diameter of 21cm which is half of the total diameter of the holder. In this case the optimal point moves towards the axis of rotation.

It is evident from the figures 10b and 10c that we must give up some of the magnitude of the ion current density to achieve a low variance in the ion current density distribution. The double ring shaped marker found in all of the figures high lights a target point offering a good compromise between the different preferred characteristics: high ion current density, small variance of the same and low sensitivity to changes in the ion beam profile. The thin solid curve in figure 11 shows the corresponding predicted ion current density distribution for the tested ion source (mean ion current density = $0.186 mA/cm^2$), whereas the thick solid curve shows the result for the reference source (mean ion current density = $0.240 mA/cm^2$). It is clearly seen how the lower order of the ion beam profile for the tested ion source is tantamount to a drop of 23 percent in mean ion current density.

The adjustment of the orientation of the ion gun could be done in the following manner. Draw the coordinate system in full scale on a piece of paper and add the double ring shaped marker. Then mirror the marker across the x-axis to obtain a drawing, which can be fixed to the mounted substrate holder with the drawing downwards and centered. Turn the substrate holder until the x-axis obtains the right orientation (the correct orientation is present when the center of the holder for the ion gun is situated on the x-axis). Finally direct the ion gun towards the mirrored marker on the drawing. We have made a special tool for this purpose. It consists of a metal-disc with a long metal rod in the center. The diameter of the metal disc is the same as the diameter of the ion gun, and it is easily fixed to the front of the ion gun during the adjustment of the orientation.

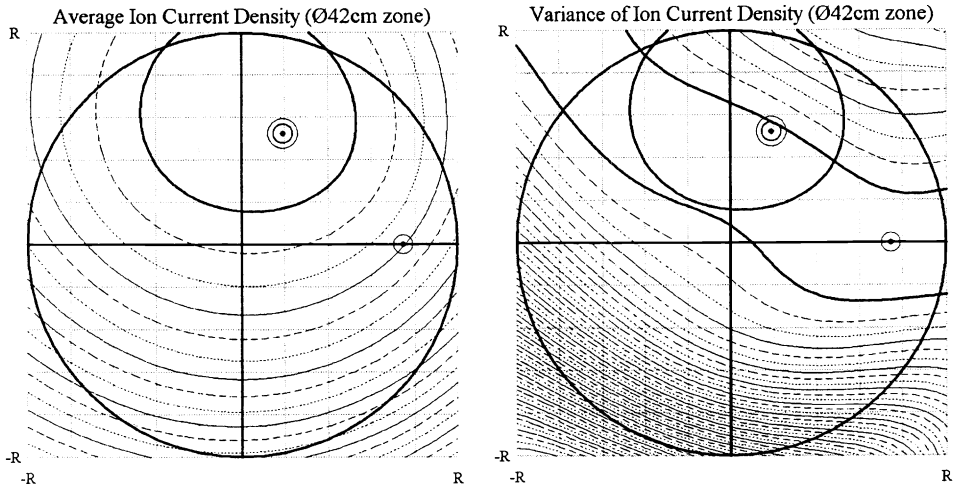

Figure 12a-b
Plots corresponding to figures 9a-b, but in this case the flat substrate holder is replaced by a calotte with a bending radius of 631.7mm. The ring shaped marker at the x-axis marks the fixed position of the holder for the ion gun.
A region with very low variance in the ion energy is observed.

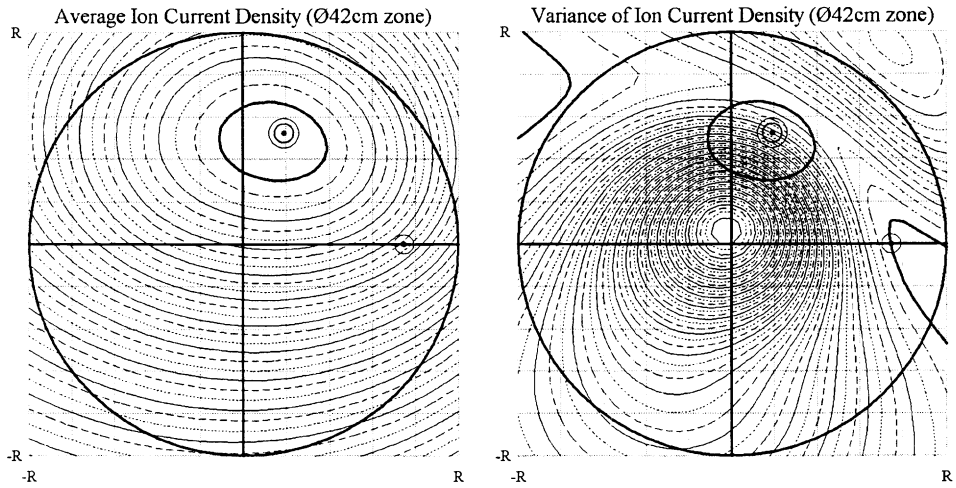

Figure 13a-b

Same as figures 12a-b but in this case the ion source has a higher ordered ion beam profile ($n \approx 3$). Thick solid circle and lines represent the rim of a calotte with a bending radius of 631.7mm and the coordinate system.

Figures 12a-b and 13a-b show the corresponding results when the umbrella shaped calotte is used instead of the flat substrate holder. Once again a double circle marker is used to mark the preferred target point and figure 14 shows the corresponding ion current density distributions. This time the predicted variance is nearly zero for the tested ion source (mean ion current density = 0.217mA/cm^2). However, once again the mean ion current density is about 26% lower as compared to the numbers for the reference source (mean ion current density = 0.296mA/cm^2).

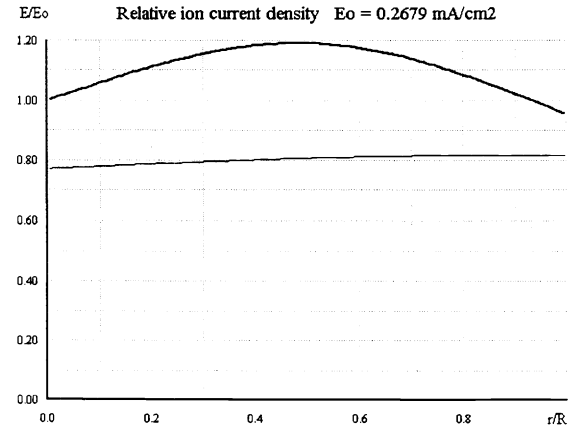

Figure 14

Curves show the predicted ion current density as obtained when the ion gun is directed towards the double ring shaped marker in the figures 12a-b and 13a-b. Thin solid curve belongs to the tested ion source (mean ion current density = 0.217mA/cm^2) whereas the thick solid curve belongs to the reference source (mean ion current density = 0.296mA/cm^2)

6. CONCLUSION

A planar ion beam probe was used for examination of the ion beam from a Mark II gridless ion source with a hollow cathode electron source. The observation that it is possible to measure the contribution from low-energy charge exchanged ions by rotating the probe at the test points gives an interesting possibility to estimate the mean free path of the energetic ions. The mean free path was nearly constant in the angular range from zero to 41 degrees and it was larger than 6.5 meters. The angular ion emission from the ion gun was described by a polynomial in cosine to the angle of emission and mathematical equations were derived describing the resulting ion current density on a flat and an umbrella shaped substrate holder. Finally a mapping technique was presented which can be used to optimize the orientation of the ion gun to achieve an even ion current density distribution and a minimal sensitivity towards changes in the ion beam profile.

7. REFERENCES

1. Henrik Fabricius and Sven Erik Schmitt, "Ion assisted deposition of oxide-materials," *DOPS-Nyt 4-1996* (The quarterly journal of the Danish Optical Society) 33–39 (1996)
2. Michael L. Fulton, "Application of ion-assisted-deposition using a gridless end-Hall ion source for volume manufacturing of thin-film optical filters," *SPIE Proceedings*, **2253**, 374–393 (1994)
3. H. K. Pulker, G. Paesold and E. Ritter, "Refractive indices of TiO_2 films produced by reactive evaporation of various titanium-oxygen phases," *Applied optics*, **15**, 2986-2991 (1976)
4. Ronald R. Willey, 'Practical Design and Production of Optical Thin Films,' Marcel Dekker Inc. New York, 1996, p.173 – 184
5. Bertrand G. Bovard, "Ion-assisted deposition," *Thin films for optical systems*, Edited by François R. Flory, Marcel Dekker Inc. New York, 1995, chapter 5
6. Henrik Fabricius, "Developments in the design and production of error sensitive smart coatings," *SPIE proceedings*, **2776**, 58-69 (1996)
7. Henrik Fabricius, "The gradient index filter: An overview," *DOPS-Nyt 4-1996* (The quarterly journal of the Danish Optical Society), 14-23 (1996)
8. A. R. Buschel, M. G. Wohlwend and M. L. Fulton, "Properties of TiO_2 and SiO_2 films prepared by Ion-Assisted Deposition using a gridless end-Hall source," *Society of Vacuum Coaters, 36th Annual Technical Conference Proceedings*, 82-87 (1993)
9. Harold R. Kaufman and Raymond S. Robinson, 'Operation of Broad-Beam Sources,' Commonwealth Scientific Corporation 1987
10. H. R. Kaufman, R. S. Robinson and W. E. Hughes, 'Characteristics, Capabilities, and Applications of Broad-Beam Sources,' Commonwealth Scientific Corporation 1987
11. Harold R. Kaufman, 'End-Hall Ion Source,' *J. of Vacuum Science and Technology A*, **A5**, July/Aug. 1987
12. Ronald R. Willey, "Some Comparisons in the application of End-Hall and Cold Cathode ion source in the conversion of SiO to SiO_2," *SPIE Proceedings,* **2262**, 14-21 (1994)
13. Ronald R. Willey, "Application of oxygen IAD using a new high-power gridless plasma source," *SPIE Proceedings* **2776**, 106-113 (1996)
14. Harold R. Kaufman and Raymond S. Robinson, 'Operation of Broad-Beam Sources,' Commonwealth Scientific Corporation 1987, p.165
15. Harold R. Kaufman and Raymond S. Robinson, 'Operation of Broad-Beam Sources,' Commonwealth Scientific Corporation 1987, p.125
16. Manual for the Mark II ion gun, Commonwealth Scientific Corporation
17. Harold R. Kaufman and Raymond S. Robinson, 'Operation of Broad-Beam Sources,' Commonwealth Scientific Corporation 1987, chapt. 7